DOE/ER 14887-3

FLUID-ASSISTED COMPACTION AND DEFORMATION OF RESERVOIR LITHOLOGIES

A.K. Kronenberg, F.M. Chester, J.S. Chester, A. Hajash,
W. He, S. Karner, and S. Lenz

Center for Tectonophysics
Dept. of Geology and Geophysics
Texas A&M University
College Station, TX 77843
(409) 845-0132

Final Report

January 2002

PREPARED FOR THE U.S. DEPARTMENT OF ENERGY
UNDER GRANT NUMBER DE-FG03-ER14887
Texas A&M Research Foundation Project NO. 441601

Start Date: 1 August 1998
Original Completion Date: 31 July 2001
Extension to: 31 January 2002
Texas A&M Research Foundation
College Station, Texas 77843

TABLE OF CONTENTS

FINAL TECHNICAL PROGRESS REPORT

Project Significance and Objectives

The compaction and diagenesis of sandstones that form reservoirs to hydrocarbons depend on mechanical compaction processes, fluid flow at local and regional scales and chemical processes of dissolution, precipitation and diffusional solution transport. While the mechanical processes that govern grain-scale compaction of sedimentary rocks in the absence of reactive fluids are well documented (*Borg* et al., 1960; *Menendez* et al., 1996; *Wong* et al., 1997), those that control time-dependent compaction and solution transfer in the presence of fluids are not (*Sorby*, 1863, *Bathurst*, 1958; *Weyl*, 1959, *Rutter*, 1983; *Pharr and Ashby*, 1983; *Bjorkum*, 1996, *Oelkers* et al., 1996; *Rezaee and Lemon*, 1996). Similarly, the solubilities of many important geochemical species in aqueous fluids at equilibrium with simple silicate minerals are known and progress has been made to evaluate reaction kinetics in fluid-rock systems in which the solids are subjected to stresses that are nearly hydrostatic and equal to fluid pressure (e.g., *Gallei and Parks*, 1972; *Rimstidt and Barnes*, 1980; *Fournier*, 1983; *Lasaga*, 1984; *Parks*, 1984; *Brantley* et al., 1986; *Applin*, 1987; *Bennett and Siegel*, 1987; *Blum and Lasaga*, 1988; *Brady and Walther*, 1990; *Brady*, 1992; *Dove and Crerar*, 1990; *Gratz* et al., 1990; *Dove*, 1994; *Dove and Rimstidt*, 1994). However, much less is known about solute concentrations in fluids that percolate through and react with solids under deviatoric stresses or about reaction and diffusion kinetics of reservoir rocks and fluids under the general conditions experienced during burial.

Observational studies of clastic reservoir rocks show large variations in porosity at similar burial depths and microstructures that reflect varying contributions of mechanical and chemical mechanisms of compaction (*Maxwell*, 1964; *Sibley and Blatt*, 1976; *Houseknecht*, 1987; *Wilson and McBride*, 1988; *McBride*, 1989; *Lundegard*, 1992; *Summa*, 1995; *Oelkers* et al., 1996; *Rezaee and Lemon*, 1996). The mechanisms of grain packing and rearrangement, and microcracking and grain crushing strongly depend on depositional loading histories. The chemical mechanisms of compaction such as dissolution at grain contacts, solute removal, and cementation within pores may depend on load histories and solution transfer at the local scale as well as on fluxes of convecting fluids. All of these processes are influenced by inherited porosities of the original sediments, grain sizes and sorting. However, much of what we know comes from qualitative observations and semi-quantitative microstructural correlations. Quantitative expressions that can be used to predict the contributions of these compaction processes are lacking.

A number of driving forces may be responsible for densification of sedimentary rocks by dissolution at grain contacts and precipitation within pores (e.g., *Magara*, 1976; *Sharp and Domenico*, 1976; *Walder and Nur*, 1984; *Meshri and Ortoleva*, 1990; *Harrison and Summa*, 1991; *Steefel and Lasaga*, 1992; *Harrison and Tempel*, 1993; *Summa*, 1995). While grain-scale solution transfer previously was the favored explanation of many investigators for quartz dissolution and precipitation within reservoir sandstones, several recent attempts to account for differences in amounts of quartz cement and quartz removed from grain contacts have relied

instead upon large fluxes of convecting fluids carrying small concentrations of silica from remote sources to sites of cementation (*Schmidt*, 1973; *Magara*, 1976; *Sibley and Blatt*, 1976; *Houseknecht*, 1987; *Wilson and McBride*, 1988; *McBride*, 1989; *Harrison and Summa*, 1991; *Land*, 1991; *Land and Macpherson*, 1992; *Harrison and Tempel*, 1993). The length scales of fluid and solute transport within sedimentary rocks are under debate, as is the extent to which deviatoric stresses within the solid play a part. To varying degrees, solution transfer may proceed over small length scales by diffusional transport between stressed grain contacts and pores, or over large length scales by convecting fluids that promote solute transport down thermal gradients and gradients in silica that stem from the occurrence of amorphous or fine-grained forms of silica, or reactions that produce silica. Without a better understanding of the mechanisms and conditions that favor grain-scale solution-transfer creep, it will be difficult to resolve these debates and to predict reductions in porosity and permeability of reservoir rocks with burial and age.

Deformation, compaction and dilation of sedimentary rocks and unconsolidated sands during short-term experiments, with or without fluids, occur by fast, brittle, frictional (isochemical brittle) mechanisms that do not depend to first order on chemical reactions. Their operation depends on non-hydrostatic stresses and effective pressures which raise deviatoric stresses to critical values at grain contacts, internal and surficial flaws, and cracks (*Zhang* et al., 1990; *Brzesowsky*, 1995; *Wong* et al., 1997). Associated mechanical properties are not strongly time- or rate-dependent. In contrast, when rocks are exposed to reactive fluids over extended periods of time, combined physical/chemical mechanisms of dissolution and precipitation reactions between fluids and the stressed solid, solute diffusion, and fluid-assisted crack growth and healing lead to solution-transfer creep, which is rate-dependent, or viscous in nature (e.g., *Elliot*, 1973; *Rutter*, 1976; *Raj*, 1982; *Pharr and Ashby*, 1983). The rate-controlling thermal activation barriers associated with compactional and distortional creep by solution transfer mechanisms lead to temperature-dependent viscosity. Just as various solution transfer mechanisms with differing driving forces compete, compaction and distortional deformation under diagenetic conditions may also occur by combinations of fast, brittle frictional and rate-dependent solution-transfer mechanisms (e.g., *Schutjens*, 1991; *Dewers and Hajash*, 1995). Thus, a transition is expected between isochemical processes that govern the short-term compaction and mechanical properties so well documented by laboratory experiments, and the solution transfer creep processes that may contribute significantly to long-term compaction and deformation of sedimentary rocks during diagenesis.

This DOE BES research has addressed fundamental mechanisms and rate laws for densification of clastic reservoir rocks by experimental and theoretical approaches. When we initiated this research, we expected to document the transition between isochemical, brittle deformation and creep by diffusive solution transfer mechanisms over a range of conditions. We expected a transition from rapid, isochemical crack growth at short times and high stress to creep compaction by fluid-assisted cracking and strain induced dissolution at longer times. In addition, we expected to document a transition from creep compaction by subcritical cracking at high stress and long times to stress-induced solution transfer creep at lower stresses and longer times as cracking becomes less significant.

We have successfully documented the transition from rapid, isochemical crack growth to time-dependent, fluid-assisted crack growth and strain-induced dissolution. However, the conditions that favor subcritical cracking and strain-induced dissolution versus stress-induced

solution transfer creep are clearly different from those we originally expected. Based on previous literature, we expected significant occurrences of fluid-assisted cracking to cease at effective pressures, P_e, less than 0.8 P_e*, where P_e* is the critical effective pressure at which rapid isochemical grain crushing leads to volume reduction. In contrast to this expectation, microstructural observations and acoustic emissions indicate that fluid-assisted cracking continues to be the principal mechanism of deformation at P_e = 0.35 P_e*. These results have implications for the range of natural conditions that favor fluid-assisted cracking, particularly as effective stresses required for this process will be even lower in the Earth as characteristic loading times are increased. They also have implications for non-equilibrium silica concentrations of percolating pore fluids, as elevated silica concentrations due to deformation are governed by increased surface areas following brittle failure rather than by stress heterogeneities and local interfacial values of pore fluid pressure, P_f.

Long-term creep experiments have been conducted on fine-grained porous quartz aggregates subjected to critical and subcritical loading conditions, at temperatures of 25^o and 150^{o}C, a fluid pressure, P_f, of 12.5 MPa, a hydrostatic effective pressure, P_e, of 34.5 MPa, and effective mean stresses (under triaxial stress states) of 2.5 to 300 MPa. The uncemented quartz aggregates are composed of sized fractions of St. Peter sand from Battle Creek, MN, and dissaggregated Arkansas Novaculite from Little Rock, AR. We have found that while the mechanical processes of grain cracking and rearrangement appear to be similar over all the experimental conditions tested, the compaction rates vary significantly and depend on the presence of a reactive fluid. Compaction rates at subcritical stress are increased from nearly unmeasurable values under dry, vented conditions to sequentially higher values as samples are exposed to water vapor, saturated with liquid H_2O, and react with a slowly percolating fluid. Silica concentrations become supersaturated with respect to equilibrium of undeformed quartz and water at the mean P_f of the experiments, and show sensitivity to flow rate, suggesting that rates of dissolution are higher than those of precipitation. We have developed a model that predicts compaction of the porous solid and composition of the pore fluid, assuming that silica enters the fluid at loaded grain contacts under open- and closed-system conditions, and that the dissolution rate depends on strain rate, strain, and stress state. Comparison of model predictions and our experimental results shows significant departures between measured fluid compositions and model predictions of transient silica concentrations. Our acoustic emissions measurements and microstructural observations suggest that reactive surfaces of newly formed cracks at grain contacts are responsible for the observed supersaturation and that cracking is dominant during long-term creep.

The Critical Envelope

The stress conditions that bound the field of time-dependent creep by fluid-assisted cracking and solution transfer processes are defined by yield envelopes for critical brittle faulting and compactive cataclastic flow (e.g., *Wong* et al., 1997). We have performed short-term experiments designed to study critical failure of uncemented aggregates of St. Peter sand and dissaggregated Arkansas novaculite. Volumetric and axial strains of cylindrical samples (19 mm diam., 38 mm length) saturated by a pore fluid of distilled-deionized water have been measured during hydrostatic and triaxial compression at room temperature and at T = 150°C using an externally heated triaxial deformation apparatus. During experiments, P_f was maintained at the same value used in our long-term experiments (12.5 MPa) and confining pressure was varied between 15 to 300 MPa to generate P_e from 2.5 to nearly 300 MPa. Throughout each experiment, we monitored pressures, pore-fluid volume, sample shortening (in triaxial tests), temperature, and acoustic emissions.

During hydrostatic loading tests, P_e was incrementally stepped and P_f was maintained constant. The volume of pore fluid exiting the specimen was continuously measured. In triaxial tests, samples were subjected to a differential stress after a target effective pressure had been established. The combined results were used to map the failure envelope for St. Peter sand at T = 25° and 150°C. P_e versus volumetric strain, β, relations also have been determined for disaggregated Arkansas novaculite samples at P_e up to ~300 MPa. However, as predicted by relationships (e.g., *Wong* et al., 1997) between critical effective pressure for grain crushing, P_e^*, porosity, ϕ, and grain size, d, P_e^* for this fine-grained (35±12μm) material could not be achieved using our apparatus.

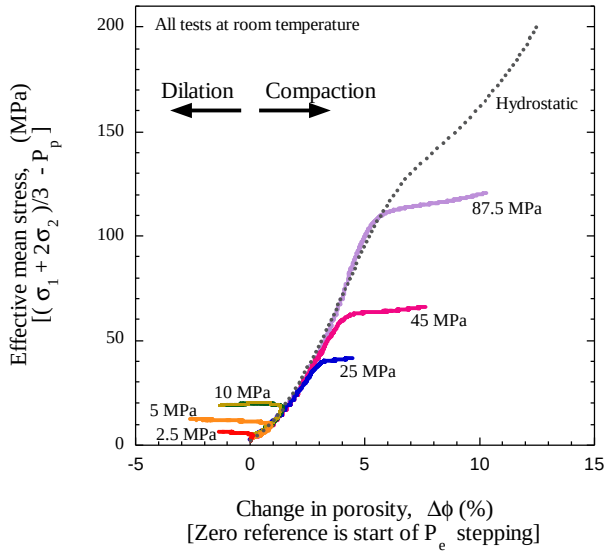

Figure 1: Change in pore volume as a function of effective mean pressure determined from room temperature experiments on St. Peter sand. Porosity is referenced to an initial effective pressure of 2.5 MPa (confining pressure 15 MPa, pore pressure 12.5 MPa). For triaxial tests, labels indicate the effective pressure prior to applying axial load to samples.

Compactional strains of samples subjected to increasing P_e exhibit a sigmoidal P_e versus porosity reduction, $\Delta\phi$, relation (Figure 1) that depends on d and ϕ. For St. Peter sand (ϕ=32% and d=255 $\pm$60 μm) at P_e < 20 MPa, strains increase significantly as P_e is increased. The rate at which porosity changes with P_e decreases, approaching a quasi-linear P_e versus $\Delta\phi$ relation over 20 < P_e < 90 MPa. Above a critical effective pressure P_e*, the change in ϕ with pressure increases again. This second transition represents the onset of pervasive grain crushing, as previously documented for fully cemented sandstones (*Zhang* et al., 1990).

Non-hydrostatic, triaxial tests show that samples deform on initial application of axial load and that subsequent yield behavior depends on the starting P_e. St. Peter sand (ϕ=32%, d=255 μm) samples begin to dilate at the onset of yielding, C', and acoustic emission, AE, rates are greater than for hydrostatic tests. Optical microscopy shows relatively little grain crushing (Figure 2) and we suspect that many acoustic emissions measured reflect frictional slip events associated with grain rearrangement. For large initial P_e (>20MPa), samples compact with yielding at C*, and AE rates are approximately 3 times the rates measured during dilatant tests, resulting from extensive grain crushing.

Data from hydrostatic tests at 150°C show a slightly lower crushing strength than at room

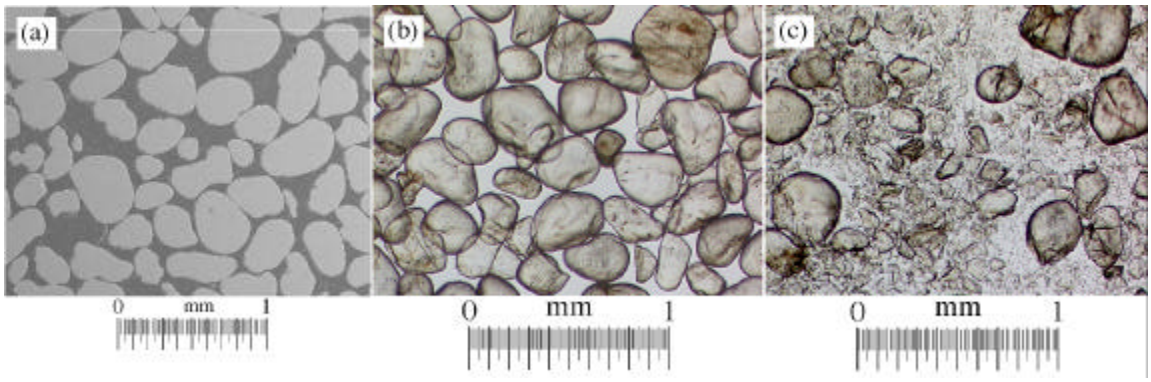

Figure 2: Photomicrographs of St. Peter sand. a) Back-scatter electron image of polished thin section of starting material. b) Transmitted light micrograph from a sample subjected to 10 MPa effective pressure followed by triaxial shortening to 10% axial strain. c) Transmitted light image from a sample subjected to a target effective pressure of 87.5 MPa, and then triaxially deformed to 10% strain.

temperature (P_e* dropping from 106 to 95 MPa), and triaxial tests at elevated temperatures show lower C* values compared to room temperature measurements. Thus, any cracking observed in long-term creep tests at T=150°C and P_e well below 100 MPa must be due to chemical reactions between the pore fluid and the solid at crack tips. Combining our results, the critical yield envelopes may be plotted in terms of differential stress versus effective mean stress (Figure 3). Samples that dilate at yield follow a Coulomb failure envelope, whereas those that compact at yield follow an elliptical envelope. Our results for uncemented quartz aggregates are in satisfactory agreement with previous results obtained for sandstones and with critical state models of soils (*Wood*, 1990; *Zhang* et al., 1990; *Lockner*, 1993; *Menendez* et al., 1996; *Read* et al., 1995; *Wong* et al., 1997; *Zang* et al., 1996; *Zhu and Wong*, 1997; *Baud* et al. 2000). However, the nonlinear mechanical response of uncemented quartz sand below critical stress states reveals the operation of non-recoverable, inelastic processes that are less prevalent in cemented sandstones. Based on the significant nonlinear response of novaculite samples that never reached critical conditions, these processes operate in relatively strong, fine-grained materials and may be

important in longer term subcritical creep tests. We plan to publish two papers on this work, one in the *Bulletin* of the *AAPG* and the other in *JGR* (*Karner* et al., in prep.).

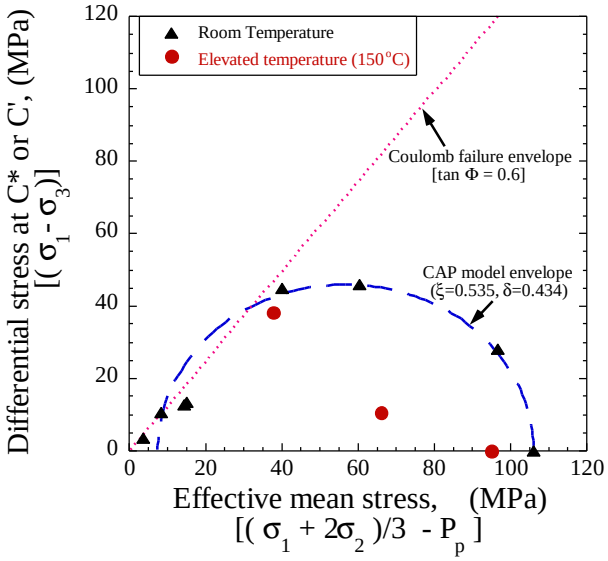

Figure 3: Yield data from the room temperature tests shown in Figure 1, and from samples deformed at elevated temperature. Elliptical yield envelope is consistent with previous results for sandstone. Increased temperature acts to depress the failure envelope.

Solution Transfer Creep Model

A number of steady-state models of diffusive solution-transfer creep have been developed, based on formulations of high temperature Coble creep and assumptions made regarding local interfacial stresses, intergranular diffusion paths, and the relative rates of diffusion and reaction at solid-fluid interfaces (e.g., *Elliot*, 1973; *Rutter*, 1976; *Raj*, 1982; *Pharr and Ashby*, 1983; *Lehner*, 1995; *Meer and Spiers*, 1997). Volumetric and axial strain rates may be calculated based on these models and known values of the effective pressure or differential stress applied, temperature, grain size of the granular material, the mean solute concentration of the pore fluid, reaction rate and/or diffusion constants, and geometrical and textural factors. However, we have not observed steady-state strain rates in any of our long-term experiments. In addition, these models do not predict the compositions of pore fluids during creep for comparison with experimental results of *Elias and Hajash* (1992), *Dewers and Hajash* (1995) or the chemistry results of our current studies.

Silica concentrations of pore fluids measured during our long-term flow-through creep experiments and at the termination of our static closed-system creep experiments reveal significant supersaturation relative to equilibrium between bulk quartz and water at the mean pore fluid pressure. *Dewers and Hajash* (1995) showed that silica concentrations during creep scale with effective pressure, and our experiments have shown that silica supersaturation is much greater under closed system conditions than under open system conditions in which pore fluids percolate across samples and remove silica. These chemical results provide constraints on the creep process much as do the mechanical results.

Motivated by these results, we have developed a model based on stress-induced dissolution, diffusive transport, and precipitation that predicts the temporal-spatial evolution of porosity and fluid chemistry during compaction of quartz sand. Adopting the *Weyl* (1959) model of dissolution and grain convergence, we kinematically relate the dissolution of minerals at grain contacts to porosity loss. In this geochemical model, we consider chemical reactions at the local scale of the solid-fluid interface, treating free interfaces at larger pores differently from solid-fluid interfaces that bound thin fluid films between loaded grains. Dissolution and precipitation are examined at free interfaces of pores, in which pore fluid pressure is assumed to equal the remotely measured fluid pressure of our pore pressure system, while dissolution is examined at loaded thin films between quartz grains. The free surface reaction rate (for dissolution or precipitation) is

related to saturation state, reactive surface area, and temperature-dependent surface reaction rate constants, while the intergranular dissolution rate is assumed to depend on stress state, strain rate, strain, grain packing (or the grain contact number), and porosity.

The total reaction rate, R, of the system can be expressed as the sum of the dissolution at grain contacts and dissolution/precipitation at free faces;

$$R = \frac{3n\, g^2 (1-f)\, b\dot{b}}{2V_m} + k_{qtz} A_{qtz} (1 - \frac{c}{c_{eq}}) . \quad (1)$$

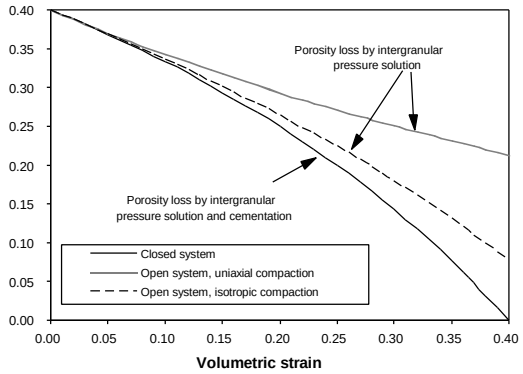

Figure 4: Porosity as a function of time for different load and flow conditions (open and closed with respect to pore fluid). Initial porosity is assumed to be 40%.

where the first term is the dissolution rate at grain contacts and the second term is the reaction rate at free surfaces, b is volumetric strain, $\dot{b}$ is volumetric strain rate, f is the porosity, n is the number of grain contacts along which dissolution occurs, g is a coefficient which depends on the stress state, V_m is the molar volume of quartz, k_{qtz} is the surface reaction rate constant, A_{qtz} is the quartz-fluid interfacial area per unit volume of porous medium, c is the mean silica concentration in the pore fluid, and c_{eq} is the equilibrium silica concentration at T and P_f of fluid in contact with unstressed, undistorted quartz. Dissolution rate is taken to be positive and precipitation rate negative.

Assuming that mass transport occurs both by advective percolation and by diffusion of ions through the fluid, mass conservation for a one-dimensional system at flow rate, v, and f is given by

$$\frac{\partial (fc)}{\partial t} - D f \frac{\partial^2 c}{\partial x^2} + v f \frac{\partial c}{\partial x} = R \quad (2)$$

$$\frac{d}{dt}((1-f)V_m^{-1}) - \frac{1-f}{1-b} V_m^{-1} \dot{b} = -R. \quad (3)$$

Expression (2) describes the temporal-spatial evolution of silica concentration in the fluid, and expression (3) describes the compaction and porosity evolution of the aggregate. Together these expressions reveal the coupling of creep, fluid flow, and mass transport.

We have simulated the compaction of quartz sandstones using these expressions and modeled geochemical transport under a variety of boundary conditions. Since porosity reduction may occur by cementation of pores as well as grain convergence, porosity does not depend solely on grain convergence and volumetric strain. Relationships between porosity and volumetric strain are illustrated in Figure 4 for isotropic and uniaxial compaction of aggregates under open system conditions and for closed system conditions. Isotropic compaction leads to more porosity loss due to intergranular stress-induced dissolution than uniaxial compaction at any given volumetric strain. Also, the difference between the results for open and closed systems increases with

volumetric strain. Intergranular dissolution is much more important in the early stages of creep, while precipitation becomes increasingly important with increasing strain.

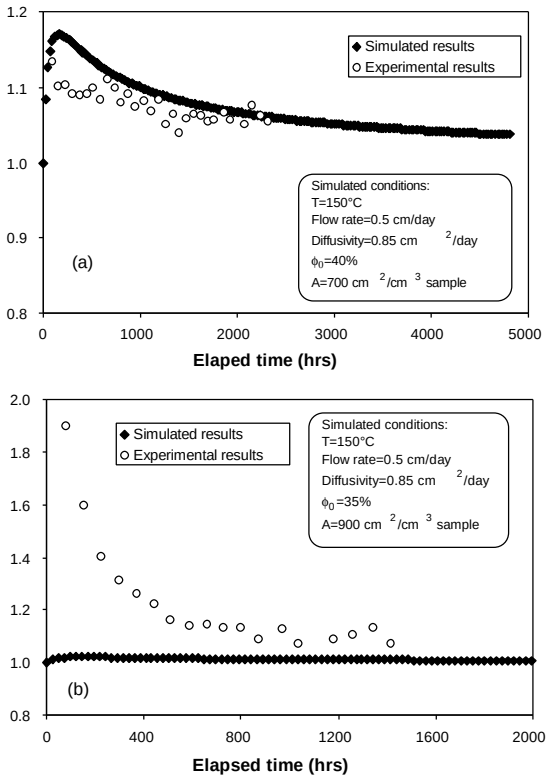

Figure 5: Comparison of experimental and simulated silica concentrations for (a) Arkansas novaculite experiment Nova-7 and (b) St Peter sand experiment Sp-44.

We also have simulated the fluid compositions exiting specimens under slow constant fluid flow rates (Figure 5). These simulations exhibit significant departures in silica concentration from equilibrium concentrations with large transients soon after effective pressure is applied, and concentrations decaying towards equilibrium values at long load times. While we have confidence in our model, given that our assumptions are met, and in the accuracy of our experimental results, comparisons of calculated and measured fluid compositions show significant departures. Measured silica concentrations do not show the large transient departures from equilibrium predicted by the model, and we suspect that the processes responsible for creep and supersaturation in our experiments differ from those assumed in our stress-induced solution transfer model.

This model and comparisons made with our experimental results form the basis for a manuscript that has been accepted for publication in the *Journal of Geophysical Research* (*He* et al., 2002a). Clearly, our original intention in developing this model was to simulate our experimental results. Yet, we have learned much more from this effort than we had expected. Rather than providing refinements in our understanding of the values of experimentally determined creep parameters, the mismatch between experiment and model suggests that very different processes operate in our experiments. At the same time, our model should be very useful to match experimental results should we succeed in activating Weyl-type stress-induced solution transfer creep in future experiments.

Long Term Subcritical Compaction Experiments

Our long-term creep compaction experiments on granular quartz aggregates subjected to T = 150°C and $P_e = (P_c - P_p)$ = 34.5 MPa (well below the critical value P_e^*=95 MPa for compactive cataclastic flow) over time periods of up to 6 months have been completed. Volumetric creep rates have been measured for specimens composed of St. Peter sand (d=255 ±60 μm and ϕ=32%) and disaggregated Arkansas novaculite (d=35 ±12 μm and ϕ=45%) under dry and wet conditions. To examine the sensitivity of deformation to the presence of H_2O as a reactive polar molecule, and as a dense fluid capable of dissolving and carrying silica by diffusion and advection, creep has been measured while samples were 1) vented to the atmosphere, 2) exposed to water vapor (P_{H2O} = 0.21 MPa), 3) saturated with a static fluid at P_f of 1.4 to 12.8 MPa, and 4) saturated with percolating fluid (P_p= 12.4 MPa) at flow rates (0.12 ml/hr) sufficiently low for steady-state silica dissolution and transport. A number of key improvements were made to obtain high quality creep results to very low strain rates. Aggregates were rigorously sealed from the confining medium using an annealed silver foil between two seamless teflon sleeves. Temperature during the experiments was held constant to within ±0.5 °C, and P_c and P_f were controlled to maintain P_e within ±0.3 MPa of the desired value. Values of β were determined from volumometer measurements of confining fluid added to the vessel at constant pressure, correcting for small fluctuations in P_c, confining vessel temperature, and room temperature. The uncertainty in β of ±0.03% reflects the remaining uncertainty in confining vessel temperature of ±0.1°C. By limiting errors and correcting for temperature fluctuations, values of $\dot{\beta}$ have been determined with a resolution of ±1 x 10^{-10} s^{-1} for measurements spanning one month.

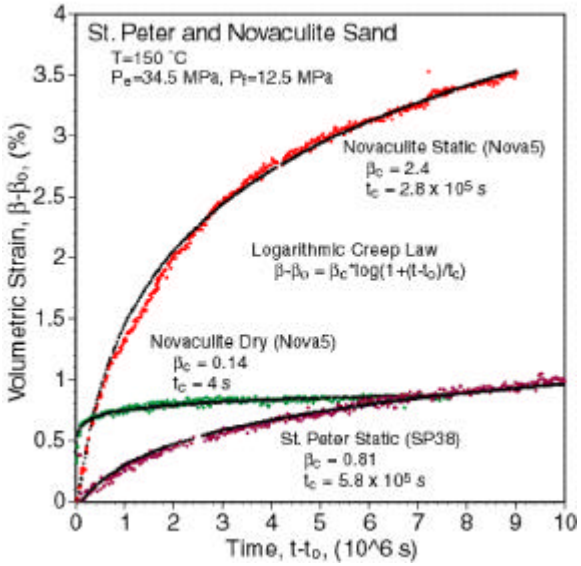

Figure 7: Logarithmic creep law fitted to creep data for St Peter sand and Arkansas novaculite

The effects of water on creep of granular quartz are illustrated by two-stage experiments (Figure 6) in which time-dependent compaction was measured first under dry, vented conditions, and then following the introduction of H_2O vapor, H_2O as a liquid pore fluid (static), or H_2O as a percolating fluid (flow). After about 1 month under load, $\dot{\beta}$ under dry, vented conditions decelerate to less than ~5 x 10^{-10} s^{-1}. Upon introduction of H_2O, creep rates show marked increases. Creep strains of samples following the introduction of liquid H_2O are greater at equal times of loading than those of samples exposed to H_2O vapor. Creep strains of samples saturated by static and percolating liquid H_2O are initially quite similar, but with time those samples subjected to percolating fluid show increasingly greater β than the closed-system experiments with a static pore fluid.

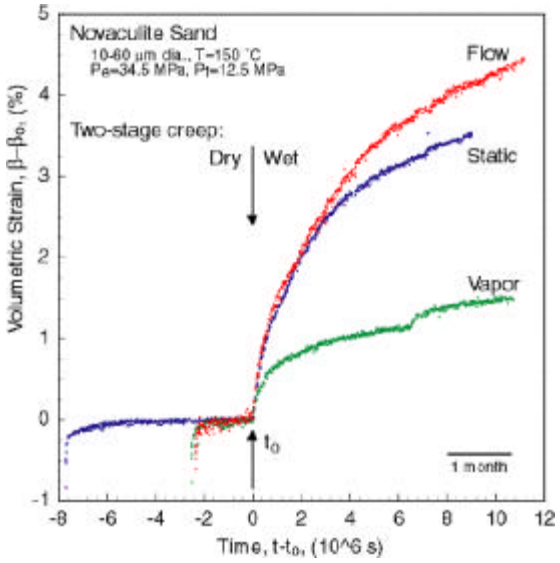

Figure 6: Long-term creep data for disaggregated Arkansas novaculite specimens under dry and wet conditions.

The pore fluid introduced to all specimens was distilled water. Previous work in our laboratory (*Elias and Hajash*, 1992; *Dewers and Hajash*, 1995) shows that silica concentrations of fluids exiting quartz aggregates at the same rates employed in the current experiments reach equilibrium silica concentrations with respect to α-quartz (160 ppm at T=150°C and P_f=12.4 MPa; *Fournier and Potter*, 1982) when P_c and P_f are equal (P_e = 0 MPa). Sequential atomic absorption measurements of fluids exiting samples during our flow-through experiments show that silica concentrations become supersaturated (Figure 5), reaching 170 ppm, and that they evolve with time under load. Fluids sampled just before the termination of closed-system experiments are highly supersaturated, reaching silica concentrations of 196 ppm. As silica concentrations of fluid increase, rates of dissolution would tend to decrease while those of precipitation would tend to increase. Thus, differences in creep rates under open- and closed-system may reflect differences in dissolution rates in response to fluid composition.

Quartz aggregates exhibit transient, decelerating creep at all experimental conditions tested. In all cases, volumetric strain data follow a simple transient creep relation (Figure 7) where strain increases linearly with the logarithm of the time since experiment conditions were established, as given by

$$\beta - \beta_o = \beta_c * \log \{ 1 + (t-t_o)/t_c \} \quad (4)$$

where t is time into the experiment, β_c and t_c are characteristic strain and time parameters, respectively, and β_o is the strain at time t_o. Overall the volumetric strain rates and time for deceleration, as given by β_c and t_c, show systematic increases with exposure to water, from low β_c and t_c values under dry, vented conditions, and increasing β_c, t_c values describing the creep of samples exposed to H_2O vapor, static liquid water, and percolating water (Table 1).

Time-dependent creep compaction of quartz aggregates vented to atmosphere (dry) shows little grain size sensitivity within the resolution of the experiments. The instantaneous volume strain upon loading appears to be greater for the finer-grained novaculite. However, the initial porosities of novaculite samples are greater than those of St. Peter sand owing to the greater angularity of the novaculite grains, and it is difficult to separate effects of porosity and grain shape from those of grain size. The transient creep of quartz aggregates under wet conditions appears to be strongly dependent on grain size. Again, isolating the effects of grain size and porosity is difficult. Nonetheless, our analyses of creep results for samples of varying

Table 1. Logarithmic transient creep law parameter fits to selected experiments.

Experiment	**Sand Type**	**Fluid Condition**	t_c **(sec)**	b_c **(%)**
SP44	St. Peter	Dry	1.7×10^1	0.08
SP43	St. Peter	Vapor	8.5×10^5	0.68
SP38	St. Peter	Static	5.8×10^5	0.81
SP44	St. Peter	Percolating	7.6×10^5	1.2
Nova5	Novaculite	Dry	0.4×10^1	0.14
Nova8	Novaculite	Vapor	6.3×10^4	0.58
Nova5	Novaculite	Static	2.8×10^5	2.4
Nova7	Novaculite	Percolating	4.2×10^5	3.1

grain size and porosity suggest that initial porosity and grain shape are not as important as grain size. In detail, grain size, porosity, and grain shape dependencies could arise from variations in grain contact dimensions, specific surface areas, and flaw sizes.

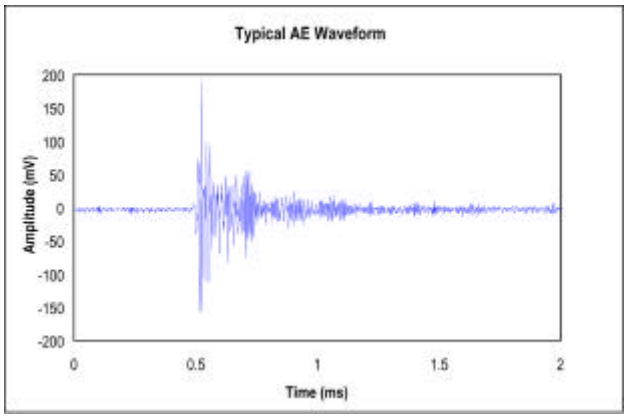

Figure 9: Acoustic emission during creep experiment.

Recasting the creep compaction data as β versus log t (Figure 8), the mechanical behavior of St. Peter sand at T=150°C and P_e=34.5 MPa are similar in short-term, wet, static experiments and long-term dry experiments. However, creep rates of fluid-saturated specimens greatly exceed those of dry specimens at experimental times greater than a characteristic time of ~10^5 seconds (or log $(t-t_o) \geq 5$), with an apparent inflection that suggests a transition in dominant strain accommodating mechanism. A similar inflection is observed in the creep data of finer grained novaculite aggregates, with creep rates of wet samples exceeding those of dry samples at shorter experimental times.

We plan to publish our long term creep data under dry and wet conditions, accompanied by fluid chemistry results in *GRL* (*He* et al., in prep.), followed by a comprehensive paper on short term and long term mechanical results, to appear in *JGR* (*Chester* et al., in prep.).

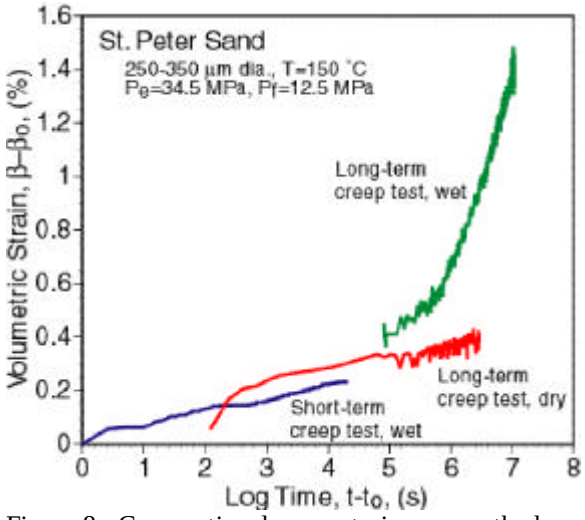

Figure 8: Compactional creep strains versus the log of time after loading for wet and dry compaction experiments.

Acoustic Emissions During Creep

The pronounced effects of fluids on long-term creep of St. Peter sand and Arkansas novaculite at a common effective pressure reveal that both chemical and mechanical processes are involved in deformation at subcritical stress levels. The low P_e applied in our long-term creep experiments relative to P_e* (e.g., P_e = 0.34 P_e*) was chosen to favor diffusive solution transfer processes relative to brittle cracking. Nevertheless, previous studies of experimentally deformed quartz aggregates indicate that multiple mechanisms may be involved, depending on the experimental conditions examined (*Sprunt and Nur*, 1976, 1977; *deBoer* et al., 1977; *Gratier and Guiguet*, 1986; *Schutjens*, 1991; *Elias and Hajash*, 1992; *Brzesowsky*, 1995; *Dewers and Hajash*, 1995). In particular, quartz sands subjected to higher stress, lower temperature conditions exhibit transgranular cracks initiated as Hertzian cracks at grain-to-grain contacts (*Schutjens*, 1991; *Elias and Hajash*, 1992; *Dewers and Hajash*, 1995). In room temperature experiments on quartz

sands, *Brzesowsky* (1995) found that uniaxial compaction was accompanied by AE. Furthermore, *Brzesowsky* (1995) found that cumulative strain and cumulative AE counts follow a nearly linear relationship.

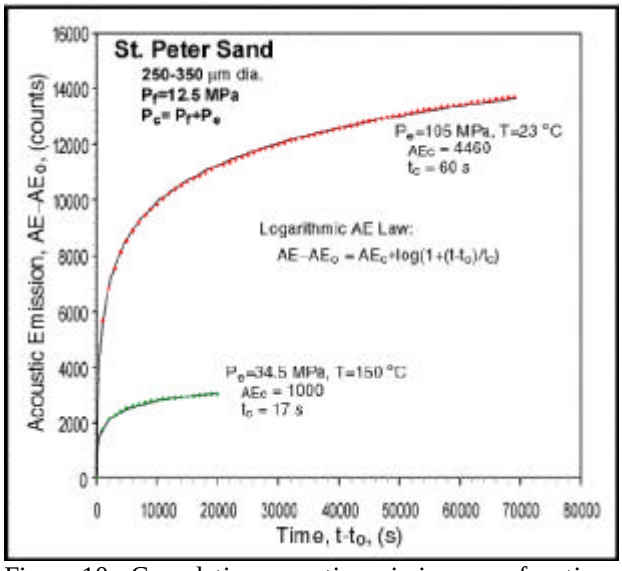

Figure 10: Cumulative acoustic emissions as a function of time during creep experiments.

One of the fundamental goals of our research has been to determine the mechanisms of deformation responsible for subcritical fluid-assisted creep. Following the lead of *Brzesowsky* (1995), we have extended the measurement of acoustic emissions up to T = 225° C and P_e = 105 MPa. These measurements, in concert with our microstructural observations, have been successful in identifying the predominant mechanisms of deformation. Our AE results require that we evaluate our creep results in terms of fluid-assisted crack propagation and pervasive subcritical grain crushing. These measurements also bear on our fluid chemistry results (Fig. 5) and on previously published measurements of time-dependent creep that were interpreted to represent diffusive solution transfer creep (e.g., *Schutjens,* 1991; *Dewers and Hajash,* 1995).

AE and β have been measured for sand (d=255 $\pm$60 μm and ϕ=32%) and novaculite (d=35 $\pm$12 μm and ϕ=45%) saturated by H_2O, and subjected to T of 25°, 150°, and 225° C, a constant P_f of 12.5 MPa, and P_e from 2.5 to 105 MPa (ie., from small to large fractions of the room temperature P_e*=106 MPa). AE are measured using a piezoelectric ceramic transducer (PZT) placed against the upper piston of the apparatus. In our AE monitoring electronics, the output of the PZT is filtered by a 4-400 kHz band pass filter and sent to a digital storage oscilloscope for waveform analysis. Each waveform captured (Figure 9) may be sent to a computer for storage purposes. The filtered signal also is rectified, integrated, and sent to a computer where individual events are counted. Volume strains were measured by monitoring the amount of pore fluid removed from the sample to maintain constant P_f during compaction under constant P_c (and constant $P_e = P_c - P_f$). Volumetric strain rates were allowed to decrease to approximately $10^{-8}s^{-1}$ before experiments were ended.

Time-dependent creep and AE events occur immediately after P_e is applied. In contrast to previous experiments on sandstones, AE are measured at very low stresses relative to critical, peak values. For dry and fluid-saturated sandstones loaded under triaxial stresses to failure, *Zang* et al. (1996) found that AE began only when stresses reached 84% (wet) and 91% (dry) of the ultimate failure strengths. Yet, for uncemented fluid-saturated quartz sand, we have detected AE at effective pressures P_e less than 10% of P_e*. Given that fluid-assisted subcritical crack growth is expected to be quasi-static, crack extension may be too slow upon nucleation to generate acoustic energy. Thus, we interpret each AE event to indicate when a subcritical crack grows to a critical length and propagation becomes unstable and rapid.

As in our long-term creep experiments, β increase with log time. Cumulative AE counts display a remarkably similar functional dependence on time (Figure 10), and at lower P_e and T, β and cumulative AE appear to be proportional. Both rates of β and AE increase with increasing

P_e; at low P_e the proportionality between β and AE is constant with time, but at high P_e and T this ratio changes with time. We interpret this to indicate that, for higher P_e and T, there is a gradual shift with time in the dominant strain mechanism from critical crack growth to time-dependent, sub-critical crack growth.

On the basis of AE and mechanical behavior, we conclude that intragranular cracking and grain rearrangement are the predominant strain mechanisms, with very little strain resulting from other diffusive mechanisms. At short times under wet and dry conditions and at long times under dry conditions, cracks that are initiated at grain contacts grow across grains, accelerating to high rates at locally critical conditions and cause AE, leading to grain collapse and compaction. At long times under wet conditions, the dominant strain mechanism gradually shifts to fluid-assisted cracking that remains subcritical during the entire process of grain failure.

These results form the basis for the Masters thesis of Stephen Lenz. We will publish our AE results and the correlation determined between AE and creep strain in *Tectonophysics* (*Lenz* et al., in prep.).

Microstructural Observations

The good correlation between cumulative AE events and cumulative strain at shorter experimental times is excellent evidence that microcracking is involved in the compaction process. However, any deficiency in AE during wet deformation, as observed at longer times may be due to slow quasi-static cracking or to other slow processes that are enhanced by fluids, such as diffusive solution transfer creep. As a result, our conclusion that microcracking is important at all conditions relies on microstructural observations. Quartz starting materials and compacted specimens have been examined by optical and scanning electron microscopy (SEM) using both secondary (SE) and backscattered (BE) electrons, with the goal of quantifying the grain size and shape distributions, the initial and final porosities, the populations of fractured grains, and fracture densities. Our microscopic observations and quantified fracture intensities reinforce the AE results. They further demonstrate that fluid-assisted cracking and grain crushing are the predominant mechanisms of deformation at T =150°C, P_p=12.4 MPa, and P_e = 34.5 MPa over all experimental times and strain rates investigated, $(t-t_0)$ up to 10^7 seconds and $\dot{\gamma}$ down to ~5 x 10^{-10} s^{-1}, respectively.

Sieved fractions of St. Peter sand and disaggregated Arkansas novaculite were examined by optical microscopy and SE SEM. Grain size and shape distributions were determined using NIH image software on ≥10 optical micrographs for each sample. The mean *d* was determined for >300 grains of each starting material, where *d* was taken to be the diameter of a spherical grain of equivalent area to that of the grain imaged; mean *d* = 35 (±12) μm for novaculite, and mean *d* = 192 (±29), 220 (±41), 255 (±60) μm, respectively, for sieved 124-180 μm, 180-250 μm, 250-350 μm fractions of St. Peter sand. Initial and final porosities were determined from BE SEM images of polished surfaces of samples that were dried and evacuated within the specimen jacket under 1 atmosphere P_e (so as to best preserve grain-to-grain contact relations) and impregnated with low viscosity epoxy. Initial porosities of individual samples varied, but porosities of all novaculite samples (~45%) exceeded those of St. Peter sand samples (~32%). These values were compared with porosity estimates based on fluid volumes extracted at the

termination of the wet creep experiments; porosity determined by these two methods are in agreement to within ±0.5%.

Qualitative inspection of experimental samples by SE and BE SEM indicates that cracking was important during creep compaction and little or no evidence has been found for dissolution or precipitation in any of the specimens compacted under dry or wet conditions. BE SEM images of the sand and novaculite starting materials show that few transgranular fractures are created during sample preparation (Figures 11a and 12a). Dry St. Peter sand samples subjected to T = 150°C and P_e = 34.5 exhibit intragranular and transgranular cracks at compactional strains of 0.4% (Figure 11b), as do dry novaculite samples subjected to the same conditions with strains to 0.8% (Figure 12b). In addition to intragranular cracks, though, novaculite samples exhibit intergranular cracks that break up multi-grain particles present in the starting material. While crack densities are significantly greater in the dry compacted samples than in their respective starting materials, much higher crack densities are observed in the sand and novaculite samples compacted to larger strains (β up to 4.4%) under wet conditions (Figures 11c and 12c, respectively). Single and multiple intragranular Hertzian cracks emanate from grain-to-grain contacts. Intergranular cracks within novaculite multi-grain particles appear to be associated with point contacts as well. In general, the number of grains displaying multiple cracks is much greater in samples deformed under wet conditions to greater strains.

The extent of microcracking has been evaluated quantitatively by determining 1) the percentages of grains that are fractured and 2) the relative intragranular crack densities of specimens loaded under dry and wet conditions to varying strains. The percentage of fractured grains in each sample was determined from the number of fractured and unfractured grains wholly contained within ten SE and BE image pairs (summing over >300 grains). Crack densities were determined as intersections of intragranular and transgranular cracks with detectable apertures along line traverses. These were used to determine specific fracture surface areas, normalizing by volume (*Underwood*, 1970; *Fredrich and Wong*, 1986). Both measures of microcracking were determined for samples subjected to T = 150°C and P_e = 34.5 MPa and varying total creep strain under dry and wet conditions, and for undeformed starting materials (prepared and placed in specimen jackets by our standard protocol).

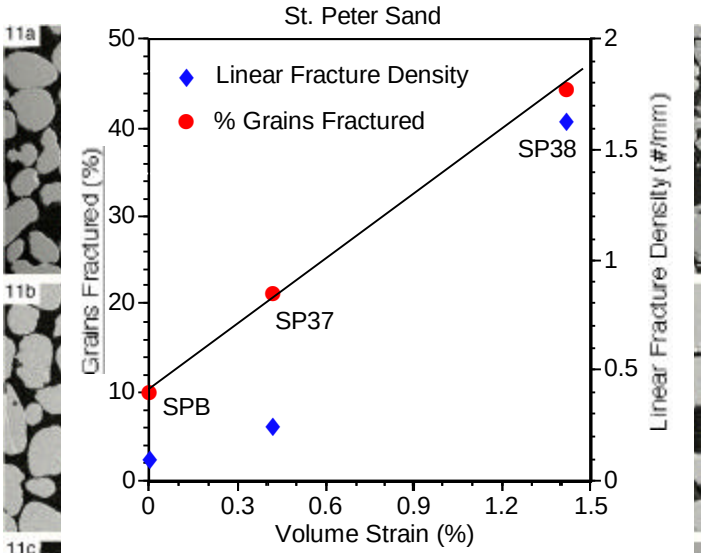

Figure 13: Percentage of grains cracked and relative crack density as a function of total volumetric strain for St Peter sand starting material (SPB) and compacted specimens, loaded dry (SP-37) and loaded dry then wet in two-stage experiment (SP-38).

Figure 11: BE SEM images of polished St Peter sand specimens (a) prior to loading, (b) loaded dry (Sp-37, T=150°C, P_e=34.5 MPa, β=0.42%), and (c) loaded under wet conditions (Sp-38, β=0.97% following dry compaction to 0.45%).

Figure 12: BE SEM images of novaculite specimens (a) prior to loading, (b) loaded dry (Nova-4, T=150°C, P_e=34.5 MPa, β=0.81%), and (c) loaded under wet conditions (Nova-5, β=3.50% following dry compaction to 0.87%).

These quantitative

microstructural evaluations suggest that intragranular microcracking, grain crushing and comminution are largely responsible for porosity reduction and creep. Samples compacted under dry conditions, and in two-stage tests in which samples were compacted first under dry and then wet conditions, show strong correlations between the measured fracture intensity and total creep strain (Figure 13). The fraction of grains fractured increases linearly with β in both sand and novaculite specimens. Fracture density increases markedly with β by some nonlinear function, which we are currently evaluating according to surface areas obtained and mechanical work done during the experiments. However, the correlations between fracture density and β are not the same for sand and novaculite samples, potentially because novaculite samples were taken to higher β and experienced more grain crushing. In addition to evidence of transgranular cracking, novaculite samples taken to large β under wet conditions exhibit large numbers of extremely fine (μm-scale), angular particles within pores. These slivers appear to be the products of brittle grain failure. Because the transgranular cracks responsible for grain failure are not identifiable after comminution and particle rearrangement, our linear fracture density measurements underestimate the extent of brittle cracking in the wet novaculite tests. We plan to publish our microstructural observations in *JGR* (*Chester* et al., in prep.), as a companion paper to that reporting our long term creep results.

Predicted Creep Compaction of Reservoir Rocks

The creep compaction laws we have determined for fluid-saturated quartz aggregates at diagenetic temperatures and pressures have important implications for porosity reduction of natural sands during burial and the quality of hydrocarbon reservoirs. Assuming that the transient laws we have determined in the laboratory extend to longer, geologic times and lower strain rates, we predict that reactive fluids during burial have profound effects on brittle mechanical processes of porosity reduction (Figure 14). Little or no porosity reduction is predicted for dry sand, while porosity reduction by fluid-assisted cracking reaches ~11% when coarse quartz sands are subjected to percolating fluids over times of 50 my. According to our logarithmic creep laws, we predict rapid early rates of compaction followed by progressively slower compaction at constant temperature and load. However, as sediments are subjected to increasing temperatures and loads during burial, actual compaction curves will be influenced both by the transient creep laws and their sensitivity to these environmental parameters.

Assuming a $\dot{\gamma}$ – P_e relationship that is linear, and an activation enthalpy for creep compaction of 70kJ/mol, the same as for subcritical, fluid-assisted cracking (*Meredith and Atkinson*, 1982; *Atkinson*, 1984), and that the creep parameter t_c varies as $t_c(P_e, T)$ while maintaining a constant β_c, we can estimate porosity reduction during burial (Figure 14b). For a burial rate of 100m/my and a geothermal gradient of 20°C/km, compaction rates are reduced at shallower depths, relative to those predicted under constant P_e and T, but are increased at greater depths. The porosity-depth curves for fluid-saturated quartz sands predict higher porosities than are typically observed for sandstone reservoirs but they have a similar form to empirical, observed porosity-depth relations (*Taylor*, 1950; *Maxwell*, 1964; *Selley*, 1978; *Baldwin and Butler*, 1985;

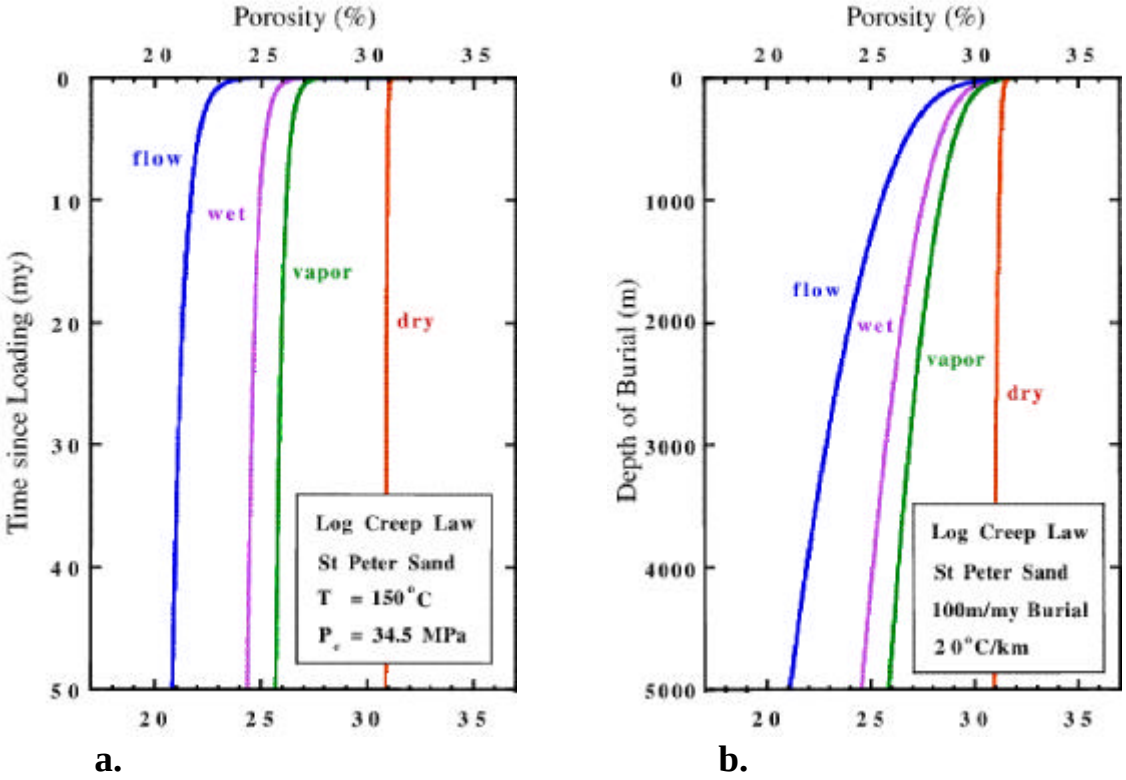

Figure 14: Predicted porosity reduction based on logarithmic creep law (4) and experimentally determined parameters for quartz sand (Table 1) (a) extrapolating to geologic times at the experimental temperature and pressure, and (b) extrapolating assuming a linear β-Pe relation, an activation enthalpy H* of 70 kJ/mol, and a natural depositional loading rate and geothermal gradient.

Wilson and McBride, 1988; *Ehrenberg*, 1993; *Bloch and Helmhold*, 1995; *Summa*, 1995). Once we determine the dependencies of compactional creep rates on temperature and effective pressure, we should be able to make realistic predictions of sand porosity reduction due to fluid-assisted cracking, in the absence of significant diffusive solution transfer and cementation. These can then be compared to observed porosity-depth relationships and interpreted in terms of the relative roles of mechanical compaction, geochemical diffusion, and cementation processes under natural conditions.

MASTERS THESES AND DOCTORAL DISSERTATIONS

Lenz S.C. (in preparation) *Subcritical Crack Growth during Compaction of Quartz Sand at Diagenetic Conditions*, Masters Thesis, Texas A&M University.

He, Wenwu (2001) *Experimental and Theoretical Modeling of Creep Compaction of Quartz Sand: Rate Laws and Evolution of Porosity and Fluid Chemistry*, Doctoral Dissertation, Texas A&M University, 90 pp.

Kwon, O. (1998) *Transport and Mechanical Properties of Saturated Wilcox Shale*, Doctoral Dissertation, Texas A&M University, 236 pp.

PUBLICATIONS

Abstracts and Oral Presentations

Karner, S.L., Chester, F.M., Kronenberg, A.K., Chester, J.S., Lenz, S.C., Hajash, A., and He, W. (2001) Compressibility and particle size effects of compacted granular quartz, *EOS Trans. AGU, 82*, F1231.

Lenz, S.C., Chester, F.M., and Karner, S.L. (2000) Acoustic emission and compaction creep of quartz sand at sub-critical stress, *EOS Trans AGU, 81*, F1131.

He, W., Hajash, A., and Sparks, D.W. (2000) Experimental and numerical modeling of creep compaction of quartz sand: evolution of porosity and fluid chemistry, *EOS Trans. AGU, 81*, F1186.

Karner, S.L., Chester, F.M., Kronenberg, A.K., and Lenz, S.C. (2000) The compactive strength of granular quartz sand, *EOS Trans. AGU, 81*, F1187.

He, W., Lang, R.A., Chester, F.M., Chester, J.S., Hajash, A., and Kronenberg, A.K. (1999) Creep compaction of quartz aggregates under dry and fluid-saturated conditions, *EOS Trans. AGU, 80*, F1020.

Hajash, A., and He, W. (1999) Creep compaction of quartz sand: effects of pore-fluid flow rates, *EOS Trans. AGU, 80*, F963.

Hajash, A., Yilmaz, R., Kronenberg, A.K., Chester, F.M., and Chester, J.S. (1998) Fluid assisted compaction of quartz aggregates at low temperature and subcritical effective pressure, *EOS Trans. AGU, 79*, F820.

Journal Publications

He, W., Hajash, A., and Sparks, D.W. (2002a) Creep compaction of quartz aggregates: effects of pore fluid flow - a combined experimental and theoretical study, accepted to *J. Geophys. Res.*

He, W., Hajash, A., and Sparks, D.W. (2002b) A model for porosity evolution during compaction of sediments, submitted to *Geology.*

He, W., et al. (in prep.) Creep compaction of quartz aggregates under dry, vapor and water-saturated conditions, planned submission to *GRL.*

Karner, S.L., et al. (in prep.) The compactive strength of granular quartz sand, planned submission to *AAPG Bulletin.*

Lenz, S.C., et al. (in prep.) Acoustic emission and compaction creep of quartz sand at elevated temperature and sub-critical stress, planned submission to *Tectonophysics.*

Chester, J.S., et al. (in prep.) Compaction creep of quartz sand, microstructures and mechanisms, planned submission to *J. Geophys. Res.*

Chester, F.M., et al. (in prep.) Compaction creep of quartz sand, mechanical data and creep laws planned submission to *J. Geophys. Res.*

Other DOE Research Published During Contract Period

Kwon, O., Kronenberg, A.K., Gangi, A.F., and Johnson, B. (2001) Permeability of Wilcox shale and its effective pressure law, *J. Geophys. Res., 106*, 19339-19353.

Kwon, O., Kronenberg, A.K., Gangi, A.F., Johnson, B., and Herbert, B.E. (in preparation) Permeability of Wilcox shale: 1. Anisotropy and effects of clay content and loading, intended for publication in *Amer. Assoc. Petrol Geol. Bull.*

Kwon, O., Herbert, B.E., and Kronenberg, A.K. (in preparation) Permeability of Wilcox shale: 2. Influence of fluid chemistry on flow and functionally connected pores, intended for publication in *Amer. Assoc. Petrol Geol. Bull.*

Kwon, O., and Kronenberg, A.K. (in preparation) Roles of fluids and volume changes on the failure of Wilcox shale, intended for publication in *Tectonophysics.*

BIBLIOGRAPHY

Applin, K.R. (1987) The diffusion of dissolved silica in dilute aqueous solutions, *Geochim. Cosmochim. Acta, 51*, 2147-2151.

Atkinson, B.K. (1984) Subcritical crack growth in geological materials, *J. Geophys. Res., 89*, 4077-4114.

Baldwin, B., and Butler, C.O. (1985) Compaction Curves, *Amer. Assoc. Petrol. Geol. Bull., 69*, 622-626.

Bathurst, R.G.C. (1958) Diagenetic fabrics in some British Dinantian limestones, *Liverpool Manchester Geol. J., 2*, 11-36.

Baud, P., Zhu, W., and Wong, T.-f. (2000) Failure mode and weakening effect of water on sandstone, *J. Geophys. Res., 105*, 16371-16389.

Bennett, P., and Siegel, D.I. (1987) Increased solubility of quartz in water due to complexing by organic compounds, *Nature, 326*, 684-686.

Bjorkum, P.A. (1996) How important is pressure in causing dissolution of quartz in sandstone? *J. Sed. Res., 66*, 147-154.

Bjorlykke, K. and Egeberg, P.K. (1993) Quartz cementation in sedimentary basins, *Amer. Assoc. Petrol. Geol. Bull., 77*, 1538-1548.

Bloch, S., and Helmhold, K.P. (1995) Approaches to predicting reservoir quality in sandstones, *Amer. Assoc. Petrol. Geol. Bull., 79*, 97-115.

Blum, A., and Lasaga, A. (1988) Role of surface speciation in the low-temperature dissolution of minerals, *Nature, 331*, 431-433.

Borg, I., Friedman, M., Handin, J., and Higgs, D.V. (1960) Experimental deformation of St. Peter Sand: a study of cataclastic flow, in: *Rock Deformation*, eds. D. Griggs and J. Handin, *Geol. Soc. Am. Mem. 79*, 133-191.

Brady, P.V. (1992) Silica surface chemistry at elevated temperatures, *Geochim. Cosmochim. Acta, 56*, 2941-2946.

Brady, P.V., and Walther, J.V. (1990) Kinetics of quartz dissolution at low temperatures, *Chemical Geology, 82*, 253-264.

Brantley, S.L., Crane, S.R., Crerar, D.A., Hellman, R., Stallard, R. (1986) Dissolution at dislocation etch pits in quartz, *Geochim. Cosmochim. Acta, 50*, 2349-2361.

Brzesowsky, R. (1995) *Micromechanics of Sand Grain Failure and Sand Compaction*, Ph.D. Dissertation, University of Utrecht, Utrecht, Netherlands, 180 pp.

Burnham, C.W., Holloway, J.R., and Davis, N.F. (1969) *Thermodynamic Properties of Water to 1000°C and 10,000 Bars*, Special Paper 132, Geological Society of America, Boulder, CO, 96 pp.

deBoer, R.B. (1977) Pressure solution: Theory and experiments, *Tectonophysics, 39*, 287-301.

Dewers, T., and Hajash, A. Jr. (1995) Rate laws for water-assisted compaction and stress-induced water-rock interaction in sandstones, *J. Geophys. Res., 100*, 13093- 13112.

Dove, P.M. (1994) The dissolution kinetics of quartz in sodium chloride solutions at 25º to 300ºC, *Amer. J. Sci., 294*, 665-712.

Dove, P.M., and Crerar, D.A. (1990) Kinetics of quartz dissolution in electrolyte solutions using a hydrothermal mixed flow reactor, *Geochim. Cosmochim. Acta, 54*, 955-970.

Dove, P.M., and Rimstidt, J.D. (1994) Silica-water interactions, in: *Silica, Physical Behavior, Geochemistry and Materials Applications*, eds. P.J. Heaney, C.T. Prewitt, and G.V. Gibbs, *Min. Soc. Amer. Reviews in Mineralogy, 29*, 259-308.

Ehrenberg, S.N. (1993) Preservation of anomalously high porosity in deeply buried sandstones by grain-coating chlorite: examples from the Norwegian continental shelf, *Amer. Assoc. Petrol. Geol. Bull., 77,* 1260-1286.

Elias, B.P., and Hajash, A. Jr. (1992) Changes in quartz solubility and porosity due to effective stress: an experimental investigation of pressure solution, *Geology, 20,* 451-454.

Elliot, D. (1973) Diffusion flow laws in metamorphic rocks, *Geol. Soc. Amer. Bull., 84,* 2645-2664.

Fournier, R.O. (1983) A method for calculating quartz solubilities in aqueous sodium chloride solutions, *Geochim. Cosmochim. Acta, 47,* 579-586.

Fournier, R.O. and Potter, R.W. (1982) An equation correlating the solubility of quartz in water from 25° to 900°C at pressures up to 10,000 bars, *Geochim. Cosmochim. Acta, 46,* 1969-1973.

Fredrich, J.T., and Wong, T.-F. (1986) Micromechanics of thermally induced cracking in 3 crustal rocks, *J. Geophys. Res., 91,* 2743-2764.

Fyfe, W.S., Price, N.J., and Thompson, A.B. (1978) *Fluids in the Earth's Crust*, Elsevier, Amsterdam, 383 pp.

Gallei, E., and Parks, G.A. (1972) Evidence for suface hydroxyl groups in attenuated total reflectance spectra of crystalline quartz, *J. Coll. Interface Sci., 38,* 650-651.

Gratier, J.P., and Guiguet, R. (1986) Experimental pressure solution - deposition on quartz grains: the crucial effect of the nature of the fluid, *J. Struct. Geol., 8,* 845- 856.

Gratz, A.J., Bird, P., Quiro, G.B. (1990) Dissolution of quartz in aqueous basic solution, 106-236ºC: surface kinetics of "perfect" crystallographic faces, *Geochim. Cosmochim. Acta, 54,* 2911-2922.

Harrison, W.J., and Summa, L.L. (1991) Paleohydrology of the Gulf of Mexico basin, *Amer. J. Sci., 291,* 109-176.

Harrison, W.J., and Tempel, R.N. (1993) Diagenetic pathways in sedimentary basins, Chapter 6 in: *Amer. Assoc. Petrol. Geol. Studies in Geology, 36,* eds., A.D. Horbury and A.G. Robinson, 69-86.

Heald, M.T. (1956) Cementation of Simpson and St. Peter sandstones in parts of Oklahoma, Arkansas, and Missouri, *J. Geol., 64,* 16-30.

Houseknecht, D.W. (1987) Assessing the relative importance of compaction processes and cementation to reduction of porosity in sandstones, *Amer. Assoc. Petrol. Geol. Bull., 71,* 633-642.

Land, L.S. (1991) Evidence for vertical movement of fluids, Gulf Coast sedimentary basin, *Geophys. Res. Letters, 18,* 919-922.

Land, L.S., and MacPherson, G.L. (1992) Origin of saline formation waters, Cenozoic section, Gulf of Mexico sedimentary Basin, *Amer. Assoc. Petrol. Geol. Bull., 76,* 1344-1362.

Lasaga, A.C. (1984) Chemical kinetics of water-rock interactions, *J. Geophys. Res., 89,* 4009-4025.

Lehner, F.K. (1995) A model for intergranular pressure solution in open systems, *Tectonophysics, 245,* 153-170.

Lockner, D. (1993) The role of acoustic emission in the study of rock fracture, *Int. J. Rock Mech. Min. Sci., 30,* 883-900.

Lockner, D., and Evans, B. (1995) Densification of quartz powder and reduction of conductivity at 700ºC, *J. Geophys. Res., 100,* 13081-13092.

Lundegard, P.D. (1992) Sandstone porosity loss - a "big picture" view of the importance of compaction, *J. Sed. Petrol., 62,* 250-260.

Magara, K. (1976) Water expulsion from clastic sediments during compaction - directions and volumes, *Amer. Assoc. Petrol. Geol. Bull.., 60* , 543-553.
Maxwell, J.C. (1964) Influence of depth, temperature, and geologic age on porosity of quartzose sandstone, *Amer. Assoc. Petrol. Geol. Bull., 48*, 697-709.
McBride, E.F. (1989) Quartz cement in sandstones: a review, *Earth-Science Reviews, 26*, 69-112.
Meer, S.D., Spiers, C.J. (1997) Uniaxial compaction creep of wet gypsum aggregates, *J. Geophys. Res., 102*, 875-891.
Menendez, B., Zhu, W., and Wong, T.-f. (1996) Micromechanics of brittle faulting and cataclastic flow in Berea sandstone, *J. Struct. Geol., 18*, 1-16.
Meredith, P.G., and Atkinson, B.K. (1982) High-temperature tensile crack propagation in quartz: Experimental results and application to time-dependent earthquake rupture, *Earthquake Prediction Res., 1*, 377-391.
Meshri, I.D., and Ortoleva, P.J. (1990) *Prediction of Reservoir Quality Through Chemical Modeling, Amer. Assoc. Petrol. Geol. Memoir 49*, 175 pp.
Nicholas, A. and Poirier, J.P. (1976) *Crystalline Plasticity and Solid State Flow in Metamorphic Rocks*, J. Wiley, New York, 444 pp.
Oelkers, E.H., Bjorkum, P.A., and Murphy, W.M. (1996) A petrographic and computational investigation of quartz cementation and porosity reduction in North Sea sandstones, *Amer. J. Sci., 296*, 420-452.
Parks, G.A. (1984) Surface and interfacial free energies of quartz, *J. Geophys. Res., 89*, 3997-4008.
Paterson, M. S. (1978) *Experimental Rock Deformation -- The Brittle Field*, Springer-Verlag, Berlin, 254 pp.
Pharr, G.M., and Ashby, M.F. (1983) On creep enhanced by a liquid phase, *Acta Metall., 31*, 129-138.
Raj, R. (1982) Creep in polycrystalline aggregates by matter transport through a liquid phase, *J. Geophys. Res., 87*, 4731-4739.
Read, M.D., Ayling, M.R., Meredith, P.G., and Murrell, S.A.F. (1995) Microcracking during triaxial deformation of pourous rocks monitered by changes in rock physical properties. II. Pore volumometry and acoustic emission measurements on water-saturated rocks, *Tectonophysics, 245*, 223-236.
Rezaee, M.R., and Lemon, N.M. (1996) Influence of depositional environment on diagenesis and reservoir quality: Tirrawarra sandstone reservoir, southern Cooper Basin, Australia, *J. Petrol Geol., 19*, 369-391.
Rimstidt, J.D., and Barnes, H.L. (1980) The kinetics of silica-water reactions, *Geochim. Cosmochim. Acta, 44*, 1683-1699.
Rutter, E.H. (1976) The kinetics of rock deformation by pressure solution, *Phil. Trans. R. Soc. London A, 283*, 203-219.
Rutter, E.H. (1983) Pressure solution in nature, theory and experiment, *J. Geological Society, 140*, 725740.
Schmidt, G.W. (1973) Interstitial water composition and geochemistry of deep Gulf Coast shales and sandstones, *Amer. Assoc. Petrol. Geol. Bull., 57*, 321-337.
Schutjens, P.M.T.M. (1991) Experimental compaction of quartz sand at low effective stress and temperature conditions, *J. Geol. Soc. London, 148*, 527-539.
Selley, R.C. (1978) Porosity gradients in North Sea oil-bearing sandstones, *J. Geol. Soc. London, 135*, 119-132.

Sharp, J.M, and Domenico, P.A. (1976) Energy transport in thick sequences of compacting sediment, *Geol. Soc. Amer. Bull., 87*, 390-400.
Sibley, D.F., and Blatt, H. (1976) Intergranular pressure solution and cementation of the Tuscarora orthoquartzite, *J. Sed. Petrol., 46*, 881-896.
Sorby, H.C. (1863) On the direct correlation of mechanical and chemical forces, *Proc. R. Soc. London, 12*, 538-550.
Spiers, C.J., and Schutjens, P.M.T.M. (1990) Densification of crystalline aggregates by fluid phase diffusional creep, in: *Deformation Processes in Minerals, Ceramics, and Rocks*, eds., D.J. Barber and P.G. Meredith, Unwin Hyman, London, 334- 353.
Spiers, C.J., Urai, J.L., and Lister, G.S. (1988) The effect of brine (inherant and added) on rheology and deformation mechanisms in salt rock, in: *Proc. Second Conf. on Mechanical Behavior of Salt*, eds., H.R. Hardy, Jr. and M. Langer, Trans Tech. Publ. Hanover, 89-102.
Spiers, C.J., Schutjens, P.M., Brzesowsky, T.M. Peach, C.J. Liezenberg, J.L.O., and Zwart, H.J. (1990) Experimental determination of constitutive parameters governing creep of rocksalt by pressure solution, in: *Deformation Mechanisms, Rheology and Tectonics*, eds. R.J. Knipe and E.H. Rutter, *Geological Society Special Publication No. 54*, 215-227.
Sprunt, E.S., and Nur, A. (1976) Reduction of porosity by pressure solution: Experimental verification, *Geology, 4*, 463-466.
Sprunt, E.S., and Nur, A. (1977) Destruction of porosity through pressure solution, *Geophysics, 42*, 726-741.
Steefel, C.I., and Lasaga, A.C. (1992) Putting transport into water-rock interaction models, *Geology, 20*, 680-684.
Summa, L.L. (1995) Diagenesis and reservoir quality prediction, *Rev. Geophys., 33 Suppl.*, 87-94.
Taylor, J.M. (1950) Pore-space reductions in sandstones, *Amer. Assoc. Petrol. Geol. Bull., 34*, 701-716.
Underwood, E.E. (1970) *Quantitative Stereology*, Addison-Wesley, Reading, Mass.
Urai, J.L., Spiers, C.J., Zwart, H.J., and Lister, G.S. (1986) Weakening of rocksalt by water during long-term creep, *Nature, 324*, 554-557.
von Damm, K.L., Bischoff, J.L., and Rosenbauer, R.J. (1991) Quartz solubility in hydrothermal seawater: an experimental study and equation describing quartz solubility for up to 0.5 M NaCl solutions, *Amer. J. Sci., 291*, 977-1007.
Walder, J., and Nur, A. (1984) Porosity reduction and crustal pore pressure development, *J. Geophys. Res., 89*, 11539-11548.
Walderhaug, O. (1994) Precipitation rates for quartz cement in sandstones determined by fluid-inclusion microthermometry and temperature-history modeling, *J. Sed. Res., A64*, 324-333.
Weyl, P.K. (1959) Pressure solution and the force of crystallization - a phenomenological theory, *J. Geophys. Res., 64*, 2001-2025.